



Tool wear of corner continuous milling in deep machining of hardened steel pocket

Wu Shixiong¹ · Li Zhiyang¹ · Wang Chengyong¹ · Li Suyang¹ · Ma Wei¹

Received: 11 November 2017 / Accepted: 3 April 2018 / Published online: 24 April 2018
© Springer-Verlag London Ltd., part of Springer Nature 2018

Abstract

Pocket molds are widely applied, whose pockets usually contain many transition corners. The machining efficiency of pocket mold can be improved significantly through deep milling. However, tools are subject to quick wear and damage during corner deep milling. Corner rounding along tool path by different approaches has great influence on the tool wear in deep milling of hardened steel pocket mold. Therefore, conducting related researches on tool wear is of practical significance. Firstly, continuous cutting pocket molds were designed for typical corners of different corner rounding approaches as per the basic theory of tool engagement angle in milling, and then hardened steel was subject to deep milling and the tool was inspected and analyzed; afterwards, tool wear process and mechanism, etc. were studied. The results showed that during the deep milling of hardened steel, adhesion, oxidation, and diffusion wear appeared gradually since the stabilization of tool wear and further aggravated along with the cutting process, which led to wear and peeling of coating as well as highly possible tool damage like tipping and chipping of tool nose in later period. It was easy to generate high tool-chip interface temperature and great tool load in the high-speed deep milling of hardened steel with small corner rounding radius. In this case, the cutting edge was under considerable thermal fatigue and mechanical shock and thus subject to extensive abrasion wear, adhesion wear, and diffusion wear. The tool wear could be reduced notably by increasing the corner rounding radius.

Keywords Deep milling · Corner · Hardened steel · High-speed machining

1 Introduction

High-speed milling is featured by high cutting speed, high feed speed and good machining quality, etc., which has been widely applied in mold manufacturing industry. There are many pocket molds in mold industries, such as automobile, aviation, and hardware mold industries. These pockets usually contain many transition corners (Fig. 1a). Multi-layer contour-parallel cutting path is a typical machining tool path for pocket molds, adopting end mill as the main tool. The side edge cutting capacity of tool can be utilized better and the machining efficiency can be improved remarkably by significantly increasing the axial cutting depth of single layer within the bearing capacity of the end mill (Fig. 1b). This machining

approach is known as deep milling [1]. Material removal rate can be improved greatly through the deep milling mode. However, in general, pocket molds are complex and diverse, and there are corners of various transitional types in the pockets (Fig. 1a). The material removed will increase suddenly in corner machining, and thus the tool load would change and increase suddenly, too. Therefore, increasing axial cutting depth further would further increase tool load and accelerate tool wear.

Hardened steel is a kind of typical difficult-to-machine material with the hardness range of 50–65 HRC, which is widely applied in molds. As for hardened steel pocket molds, when cutting depth is increased, both milling force and temperature would increase, which may lead to rapid wear and even breakage of tools, especially in deep milling of corners. For this reason, carrying out researches on the tool wear in deep milling of corners of hardened steel pockets is of practical significance for controlling tool loss, improving deep cutting capacity and enhancing machining efficiency.

The cutting state between tool and work-piece changes from relatively stable to abruptly drastic, which is the root

✉ Wu Shixiong
151688386@qq.com

¹ Mechanical and Electrical Engineering Institute, Guangdong University of Technology, Panyu Higher Education Mega Center, Guangzhou 510006, China

cause of the corner machining problem. The cutting state of corner can be analyzed with engagement angle. According to the engagement angle model of Choy and Chan [2] and the corner milling force calculation of Han and Tang [3], the change of engagement angle is very closely related to tool load and wear. If the range of engagement angle in the milling process can be effectively controlled, the tool load can be controlled and the tool wear can be substantially reduced, so that a more stable machining process can be ensured. There are two existing corner milling methods: varying movement parameters and varying machining paths. The method by varying movement parameters is mainly to adjust and control speed, acceleration, and other parameters in the process of machining. Bae et al. [4] presented a simplified-cutting force model to adjust the feed rate and control cutting-load in high-speed pocket machining. Karunakaran et al. [5] developed an octree-based NC simulation system to predict cutting forces and optimize the cutting parameters such as feed rate and spindle speed. Liu et al. [6] proposed a feed rate optimization method with several constrains, and their experimental results indicated that the optimized feed rate can satisfy the requirements for pocket milling. The second method is mainly to change the tool path in order to control the cutting state of tool and workpiece. Choy and Chan [2, 7] adopted a series of bows to remove progressively the high amount of material at corners. In their approach, the cutting load and vibration were reduced effectively. Zhao et al. [8] inserted biarc curve for cornering cut and claimed that the residual material can be removed effectively. Ibaraki et al. [9] presented a trochoidal approach to remove the materials of sharp corners and narrow slots. Their experiments demonstrated an obvious improvement of tool wear. Dumitrache and Borangiu [10] presented a NC tool-path generation strategy with tool engagement control for arbitrarily complex discrete part geometry and concluded that it can reduce machining time and tool wear in high-speed machining. The second method is easier to be applied, with less dependence on CNC system. Corner rounding process in tool path generation can effectively control and improve the cutting state of tool and workpiece, reducing the radial cutting depth and tool load in the corner milling. Corner rounding process is simple and practical, and can be attributed to the second method. And it is often used in generating high-speed milling tool paths. In addition, CNC system may change the corresponding acceleration and deceleration ability, so corner rounding treatment is also featured by the first method. When machining the pocket of a hardened steel mold in the high-speed deep milling mode, corner rounding is still a very effective way to deal with machining problems. Different corner rounding methods may all have strong impact on the control of the abrupt change machining load, reducing the tool wear and preventing the breakage of tool while milling the hardened steel pocket. Therefore, the study of the tool wear process, tool wear causes, and

mechanism of the corresponding machining bears important application value. Based on these conditions, an in-depth study will be made on the tool wear of corner continuous milling in the high-speed deep machining of hardened steel pocket.

Several scholars have made tool wear studies on the tool wear of coated carbide tools in the hardened steel high-speed milling. Dolinšek et al. [11] used a cutting tool with a diameter of 6 mm to mill-hardened and tempered steels of hardness over 50 HRC. They found that abrasion wear, high temperature oxidation wear, and adhesion wear were the major causes of tool coating wear and tearing. Ghani et al. [12] found that the micro-chipping and the peeling of coatings occurred because a high feed rate and a large depth of cut led to tool wear during the high-speed milling of hardened steel and flank wear was determined to be the main cause of tool wear. Liao et al. [13] studied the high-speed milling of NAK80 hardened steel with the minimum quantity lubrication (MQL) and affirmed that the thermal cracks, oxidation wear, and adhesion wear were reduced effectively. Wang et al. [14] used two types of PVD-coated carbide tools (TiAlN and TiSiN) to determine the mechanism of cutting tool wear when high-speed machining of hardened steel. Their experimental results indicated that the

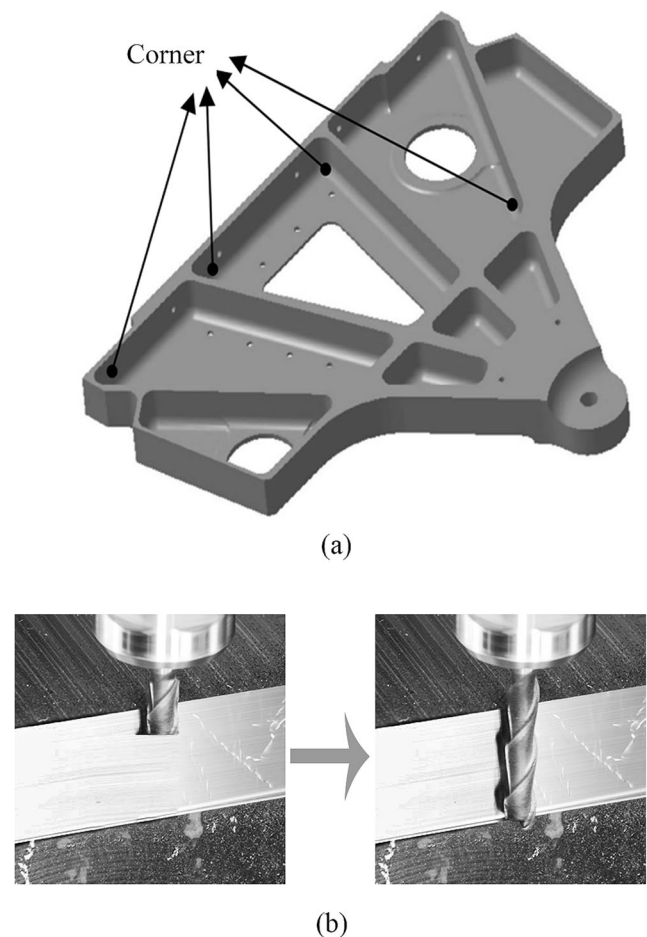


Fig. 1 High-speed deep milling of pocket mold: **a** pocket mold with multiple transition corners and **b** deep milling

dominant wear patterns of coated carbide tools included flank wear, rack face wear, breakage, and micro-chipping. In a high-speed milling study performed on H13 hardened steel using a PVD-coated cemented carbide tool, Machado and Diniz [15] concluded that the attrition followed by microchipping of the cutting edge were the wear mechanisms at the portion of the cutting edge that removed thin chips, and diffusion and attrition followed by microchipping were the wear mechanisms at the part of the cutting edge that removed thicker chips. Braghini and Coelho [16] presented a wear mechanism study of PCBN tools when end milling hardened steels at low/medium cutting speeds. The experiments showed that the minimal wear mechanism was a combination of adhesion and abrasion. Cui et al. [17] found that the tool life of CBN tool of high-speed face milling increased with radial depth cut and then decreased for most of the selected cutting speeds. In addition, the tool wear in high-speed milling of hardened steel is strongly correlated with the dynamics, chip morphology [18], and surface quality [19]. According to the research of high-speed milling of hardened AISI A2 steel from Pu and Singh [20], PCBN tools produced better surface finish because of less tool wear and damage. Wojciechowski et al. [21–23] conducted a series of milling researches about hardened steel and their results indicated that the surface finish and tool life was improved by optimizing milling forces and machining parameters.

Among the above studies, there are few on the tool wear associated with high-speed deep milling. In addition, the existing tool wear research on the milling or turning of hardened steel generally considered the steady state of the processing conditions, that is, the cutting material keeps constant every unit time. In the study of milling tool wear, the steady-state machining conditions refer to the row milling or contour-parallel milling, and the engagement angle keeps constant during machining. There are very few literatures on the research of tool wear in an unsteady machining condition. Qin et al. [24] discussed the variable radial depth of cut machining in the turning of ceramic cutting tools, and showed that the variable radial depth could deeply affect tool wear. This paper deals with the study of deep milling in different corner rounding radius. It is essentially a machining process of variable radial depth, which is a kind of non-steady-state processing. As far as we know, there is no corresponding research about the tool wear of deep milling of hardened steel in the non-steady cutting state.

Since researches on the wearing process and mechanism of corner cutting tools in deep milling of hardened steel pocket are of application significance, specialized scientific researches are made in this paper. In addition to corner rounding radius, changes in cutting depth may also have certain impact on the tool wear of deep milling of hardened steel pocket. Therefore, such two factors are associated for researches. Discussions are made from the following aspects: part 2 introduces the design, machining methods, and processes of

experiment schemes; part 3 analyzes and discusses the experiment results; part 4 gives out the conclusions.

2 Experiment procedure

Firstly, the geometrical features of different corners rounding modes are analyzed. Secondly, the experimental scheme is designed. Finally, the experimental processing equipment, processing conditions, and test methods are introduced.

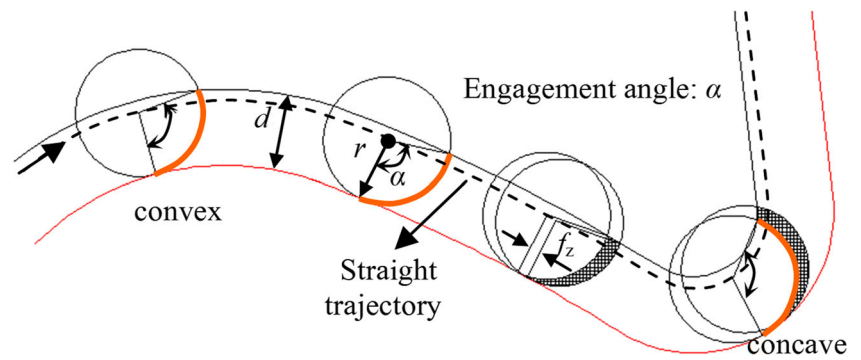
2.1 Geometrical analysis

Considering that engagement angle reflects the cutting geometrical relationship between tool and work-piece and represents the change characteristics of cutting load, the engagement angle is taken as the entry point for basic analyses of geometrical characteristics of corners subject to different corner rounding approaches.

Figure 2 is the schematic diagram of corner milling. Engagement angle α keeps changing when the tool moves along the tool path shown as the dotted line. When it enters the concave corner area, change in engagement angle increases suddenly, and both the material cutting amount and tool load change abruptly [7]. The engagement angle is maximized at certain position in the concave corner, when the tool load will reach the maximum value, too. The corresponding calculation method of engagement angle can be consulted in the literature of Wu et al. [1].

Different corner rounding approaches may have great influence on the tool wear in corner milling. Geometrical analysis will be made for corners of different corner rounding radii from the aspect of engagement angle changes. Then, 30–90° corners occur frequently in actual production and machining of pocket molds which have great influence on machining. Typical 45° corner is selected here for corner machining researches. Figure 3a is the general schematic diagram of geometrical change in corner engagement angle, where point O is the center of tool circle, f is the feed direction, path U is the path of the center of tool circle last time, path V is the path of the center of tool circle this time, and the distance between tool path loops is $d=0.5$ mm, which is commonly used in actual machining. A tool circle radius is offset for paths U and V respectively to obtain PU and PV and facilitate calculation of changing engagement angles. In this case, milling feed of the tool with the center of tool circle along path V is equivalent to rolling milling feed of the tool with the tool circle along path PV . Analyses are made for small corner ($r=1$ mm), medium corner ($r=8$ mm), and large corner ($r=25$ mm) respectively in Fig. 3b–d. Take Fig. 3b as an example for explanation. The tool path is straight before feeding to O_1 along path V , and the engagement angle α_1 is 28.9°. The tool enters the corner area from O_1 to O_3 , in which the engagement

Fig. 2 Changes in engagement angle during pocket milling



angle gradually increases to the maximum value 108.7° from 28.9° with an increase of 276.1%. Afterwards, the engagement angle gradually reduces to 28.9° from 108.7° , and the corner area is cut out in the process that the tool circle moves to O_5 from O_3 .

The results below are obtained by sorting out the analysis results of Fig. 3b–d:

(1) Small corner rounding radius approach ($r = 1$ mm, approach A): the change process of engagement angle is $28.9^\circ - 108.7^\circ - 28.9^\circ$. The changing amplitude of engagement angle is so large that it reaches 276.1% with great load change.

(2) Medium corner rounding radius approach ($r = 8$ mm, approach B): the change process of engagement angle is $28.9^\circ - 57.5^\circ - 28.9^\circ$. The changing amplitude of engagement angle is 98.9%.

(3) Large corner rounding radius approach ($r = 25$ mm, approach C): change process of engagement angle is $28.9^\circ - 31.5^\circ - 28.9^\circ$. The change of engagement angle (9%), as well as the load, is very small. Conventional milling path with relatively constant engagement angle takes up a large proportion in the pocket contour-parallel cutting paths. Approach C of corner in Fig. 3d is very close to such path, thus its tool wear characteristics are similar, too.

Fig. 3 Variation process of the engagement angle of different corner rounding modes: **a** general schematic diagram of the engagement angle change at corner, **b** small corner rounding modes ($r = 1$ mm, approach A), **c** medium corner rounding modes ($r = 8$ mm, approach B), and **d** large corner rounding modes ($r = 25$ mm, approach C)

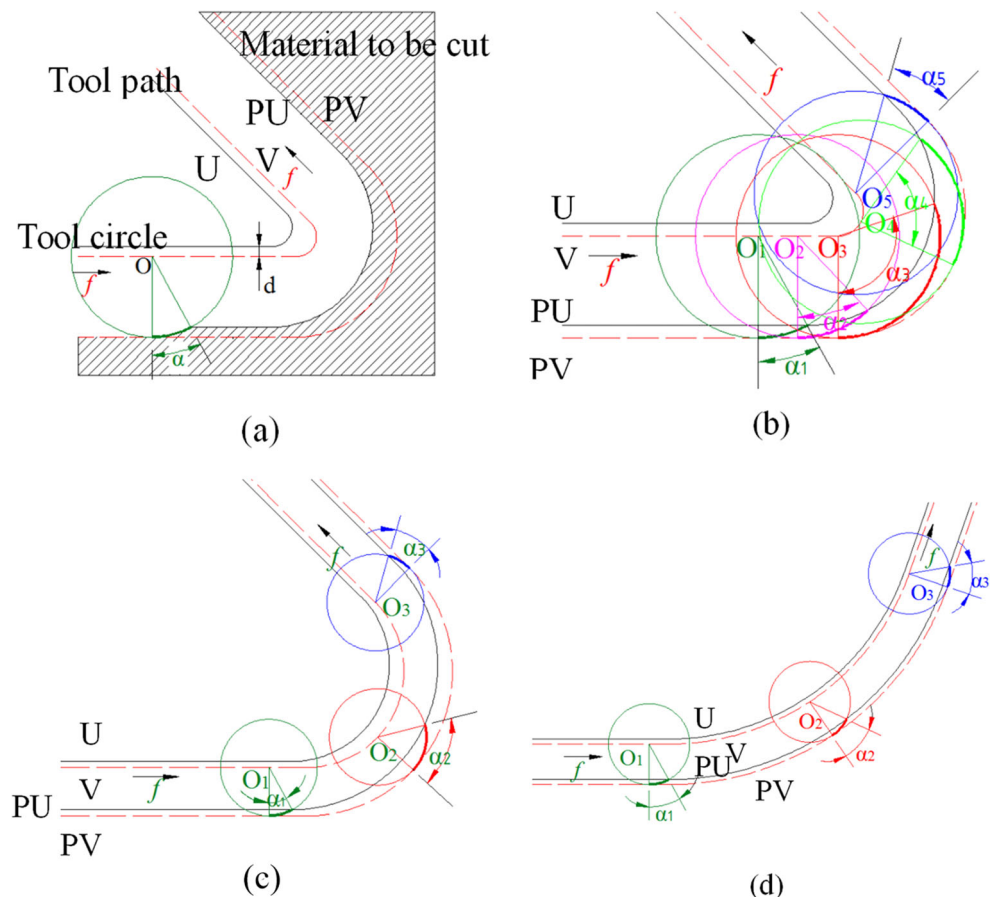
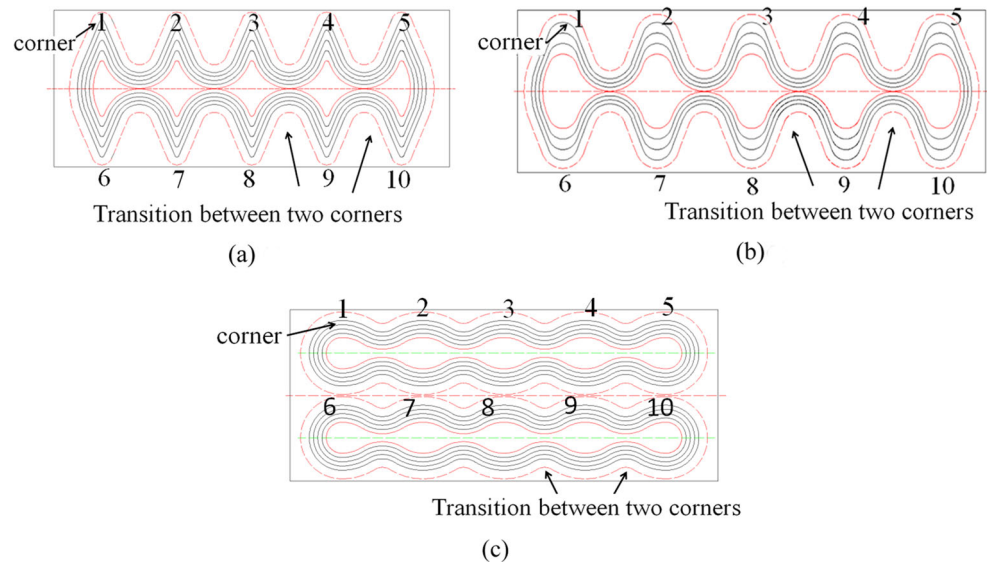


Fig. 4 Corner continuous cutting paths of three different corner rounding approaches (45° corners and 0.5 mm circle distance): **a** small corner rounding modes ($r = 1$ mm, approach A), **b** medium corner rounding modes ($r = 8$ mm, approach B), and **c** large corner rounding modes ($r = 25$ mm, approach C)



2.2 Experiment scheme

Corner paths can be mainly classified into continuous feeding paths and intermittent feeding paths in actual milling of mold pockets. However, most machining paths are continuous, i.e., corner paths and peripheral paths are connected continuously instead of intermittently. The path in corner cutting experiment needs to be designed into continuous path to simulate this cutting condition, which is the key of design.

Corner continuous cutting paths of three different corner rounding approaches are designed on the basis of geometrical analysis of changes in the corner engagement angles above, shown as Fig. 4. Ten corners are designed in each approach, adjacent corners are connected through smooth arc path, and the change in the engagement angle of the connecting path is basically constant. The number of corner paths accounts for more than 80% of the total paths, while that of connecting paths accounts for less than 20% of the total paths, which ensures that the machining results are subject to corner paths. Climb milling from inside to outside is adopted for machining. The internal material of the innermost ring (red) is removed by other tools in advance of the cutting contrast experiment.

In addition to corner rounding radius, different axial cutting depths may also have great influence on the tool wear in high-speed deep milling of corner. Therefore, axial cutting depth needs to be taken into account in the experiment design. Two large axial cutting depth values, i.e., 7 and 12 mm, are considered in the experiment. A double-factor test is designed finally, see Table 1 for details. Actual machining experiments are carried out for each combination respectively on the premise of ensuring that other cutting parameters are the same.

2.3 Machining and test

The high-speed milling test is carried out on the DMU-60T machining center. The spindle motor power of this machine is 15 kW, and its maximum speed is 24,000 r/min. The maximum feed rate of the worktable can reach 26 m/min, and this machine operates on Heidehain iTNC 530 numerical control systems. The experimental device is the same as that used in Wang et al. [25], shown in Fig. 5, and featured a heat-shrinkable extended handle. Dry cutting conditions are employed.

One new tool is used for actual machining on the high-speed machine for each combination in the experiment schemes listed in Table 1 to test force, temperature, tool wear, and other factors. Solid carbide four-flute flat end mill with the model of HMX-4E-D8.0 manufactured by Zhuzhou Cemented Carbide Cutting Tools Co., Ltd. is selected for machining. The rake angle and helix angle of the tool is 5° and 45° respectively. The tool surface is applied with superhard nano-coating. It can be learnt from measurement before experiment that the element contained in the tool coating and in the carbide substrate of the tool is Ti,Al,Si,N and C,W,Co respectively. The workpiece tested is made of P20 steel, with a dimension of $35 \text{ mm} \times 80 \text{ mm} \times 400 \text{ mm}$. P20 steel enjoys good hardness and machinability, which is suitable for large and medium-sized precise molds. The hardness of the pre-hardened P20 steel is HRC 30–42. Pre-hardened steel can be hardened by quenching plus low-temperature tempering to improve mold life. The hardness after quenching can reach 50–54 HRC. Contour-parallel cutting from inside to outside of the pocket, climb milling, and high-pressure air cooling are selected for the milling in the experiment. Major machining parameters are shown in Table 2.

Table 1 Experimental program

Factor 1 (different corners rounding)	Factor 2 (axial cutting depth A_p , mm)	
	$A_p = 7$ mm	$A_p = 12$ mm
Approach A ($r = 1$ mm)		
Approach B ($r = 8$ mm)		
Approach C ($r = 25$ mm)		

Measurement of tool flank wear and establishment of tool wear curve are major tasks in the tool wear experiment. OLYMPUS-SZ61 stereo microscope is used to observe the wear zone on the tool flank of the cutting edge at half axial cutting depth and measure tool wear (see Fig. 6). ISO standard is selected as the tool blunt standard, namely the critical value for wear on the tool flank is $VB = 300 \mu\text{m}$. For the micro-scale effects of tool wear and breakage, a NanoSEM430 ultra-high resolution field emission scanning electron microscopy is used for further meticulous observation. In addition, milling force and temperature are involved in tool wear experiment. Kistler9257B 3-axis dynamometer is used to collect and record milling forces, and TVS-500EX type thermal infrared imager is used to collect and record the temperature of the milling area.

3 Experiment results and discussion

3.1 Tool wear process of deep milling of hardened steel in the non-steady cutting state

Generally, the wears on the tool flanks of different cutting lengths are recorded and tool wear curves are established on

this basis with unchanged radial cutting depth of tool and stable machining conditions in most tool wear researches. The radial cutting depth of tool is variable in continuous milling of corner. Therefore, the tool wear curve described by cutting length is subject to certain limitation. In this paper, the wears on the tool flanks of different material removal amounts are recorded and tool wear curves are established on this basis to reflect the wear change degree more accurately.

Machining and test are carried out for each combination in Table 1 respectively. Measure the wear on the tool flank once after machining of each pocket tool path loop (see Fig. 4) to obtain a coordinate point, and then connect the coordinate points smoothly to obtain the tool wear curve. Figure 7a, b shows the final tool wear curves. In addition, a visual contrast analysis is made for the tool flank wear maps of the three approaches. Namely, corresponding material cutting amount is recorded when blunt standard is reached in approach A, and the tool flank wear is measured once at corresponding material cutting amount in approach B and approach C. In this way, Fig. 7c, d is formed.

According to the variation in tool wear, the tool wear process can be divided into three stages, the initial wear, the stable wear, and the sharp wear. In the initial tool wear stage, the surface of the tool is rough, the interface between the tool and workpiece and the interface between tool and chip are small, the stress near the cutting edge is large, and the wear is fast. In the stable wear stage, the wear zone will increase gradually. Some material of the chip is gradually bonded to the cutting edge to form adhesive wear, which will gradually become serious and some of the adhesive blocks may be peeled off to form pits. In addition, the tool nose of the cutting edge area

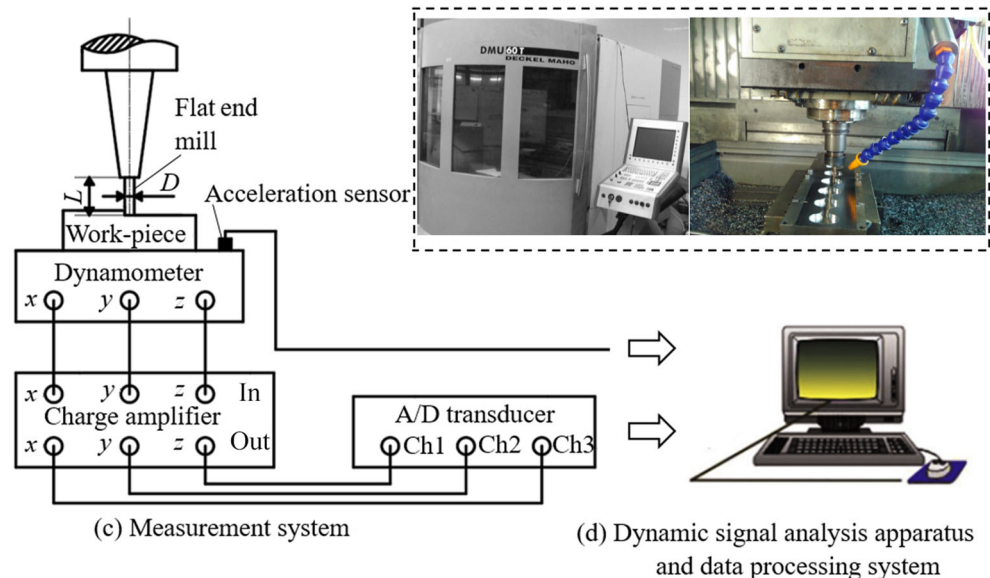
Fig. 5 Schematic of high-speed milling experiments

Table 2 Conditions of tool wear experiments

Coating of cutting tool	Tool matrix material	Workpiece material P20	D (mm)	V_c (m/min)	f_z (mm/z)	A_p (mm)	A_c (mm)
Ti, Al, Si, N	C, W, Co	Fe, Cr, C, Mn, Mo, Si, P, S, V, etc.	$\phi 8$	150	0.025	12 or 7	0.5

wears out more rapidly, the coating starts to peel off, and the chipping from the mechanical shock gradually emerges. In the rapid wear stage, the blade becomes blunt, the cutting force and temperature increase, the wear rate increases rapidly, and the wear curve slope is larger. In addition to severe adhesion wear, oxidation wear and diffusion wear are also formed because of high temperature, which results in fast coating peeling and exposure of tool matrix. Due to serious chipping in the tool nose of the cutting edge area, the cutting blade may break.

Further analysis is made for Fig. 7. In corner rounding approach A, the stable wear stage is very short, and the rapid wear stage comes very soon. Black adhesive material and peeling of a part of coating can be seen on the tool flank, serious wear and tipping occur at tool nose, and the tool life is reduced. In corner rounding approach B, the stable wear stage is relatively longer, and the final tool life is longer than that in approach A, too, which indicates that wear can be reduced by increasing corner moderately. Compared with the two approaches above, in corner rounding approach C, the slope at initial wear and rapid wear stages is smaller, while the stable wear stage is longer, but the width of wear zone, coating condition, and tool nose breakage degree are obviously better than that in approach A and B; therefore, the tool life is further improved. The situation above shows that increasing corner rounding radius has very obvious effect on reducing tool wear.

3.2 Milling force and temperature in tool wear

Hardened steel materials exhibit high hardness and good wear resistance. In the high-speed deep milling of hardened steel, much energy will be consumed to shear the workpiece materials to form the chip, and the friction and squeeze between the

chip and tool are serious, which results in larger milling force, more heat and higher tool temperature, and speeding-up of the tool wear process.

3.2.1 Milling force

Component forces in three directions— F_t , F_f , and F_z —can be measured with the milling force platform. Since multiple continuous corners are involved in the machining of each experiment, adopting resultant milling force can facilitate comparative analysis of milling forces. Therefore, forces in three directions are composited by the compositing function of the force-measuring software in data processing, i.e.,

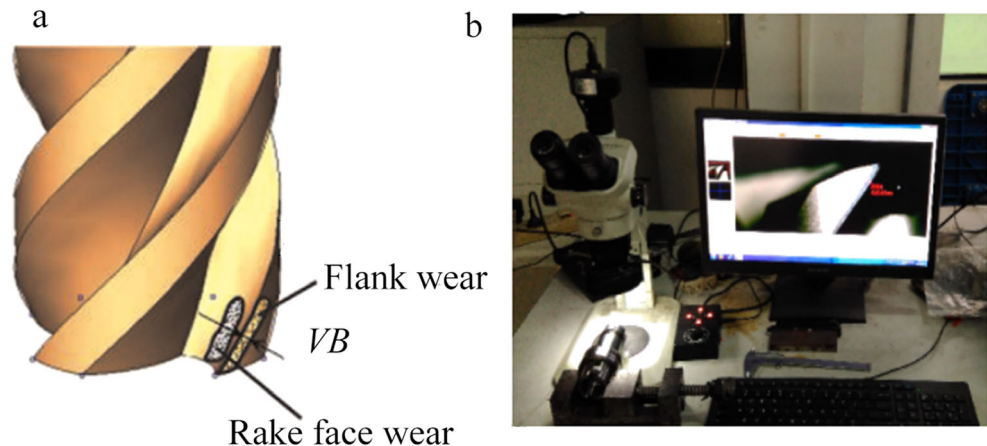
$$F_r = \sqrt{(F_t^2 + F_f^2 + F_z^2)} = \sqrt{F^2 + F_z^2} \quad (1)$$

where F_t and F_f are horizontal forces and F_z is the vertical force, respectively.

Axial cutting depths of 7 and 12 mm are adopted for three corner rounding approaches respectively, and the milling force test results are shown as Table 3. As for the three corner rounding approaches, drastic change in milling force occurs at the corner in small corner rounding approach A, and the tool is subject to damage and machining chatter; change in milling force at the corner in large corner rounding approach C is very gentle, which is beneficial to tool protection and stable machining; the performance in medium corner rounding approach B is between that in approach A and approach C.

The maximum milling force is found out based on Table 3 and the average milling force is figured out, and then, the histogram shown as Fig. 8 is established. It can be learnt from Fig. 8 that the sequences of the maximum values and average values of the milling force at corners in three corner rounding

Fig. 6 Tool wear test: **a** tool wear of major cutting edge and **b** stereoscopic microscopy



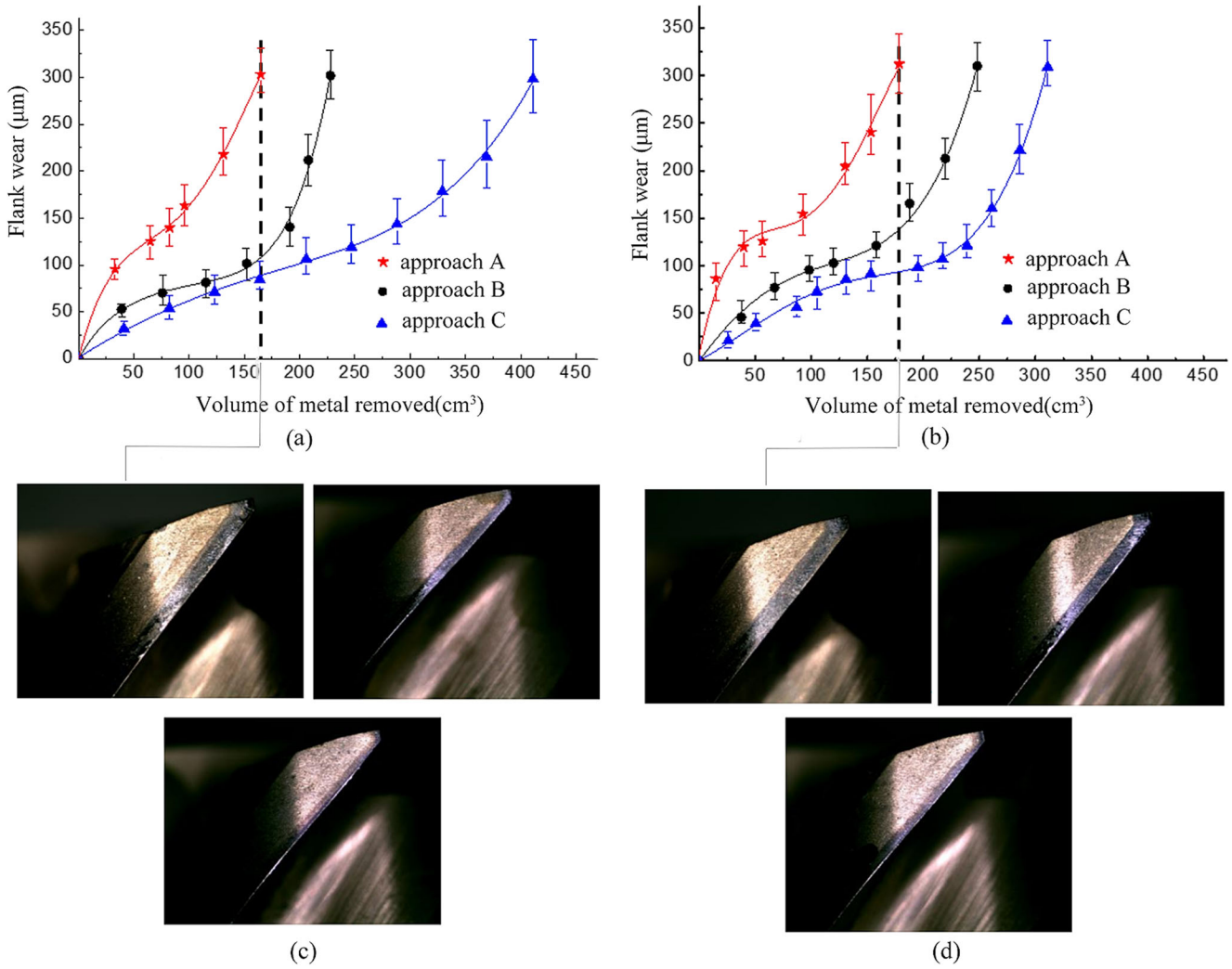


Fig. 7 Tool wear comparison on deep milling of hardened steel pocket in three corner rounding approaches: **a** contrast of tool wear curves with axial cutting depth $A_p = 7$ mm, **b** contrast of tool wear curves with axial

cutting depth $A_p = 12$ mm, and **c, d** comparison of tool flank wears of three approaches relative to vertical lines

approaches are “approach A > approach B > approach C” for axial cutting depths of 7 and 12 mm, and there is significant difference in the milling force values of three corner rounding approaches. In the following section, this phenomenon will be explained by means of material removal rate, force balance, chip formation, and chip morphology.

The corner engagement angle analysis results in Section 2.1 suggest that a small corner rounding radius can lead to great change in engagement angle. The difference in engagement angle is the root cause of the change in milling force [26]. The maximum corner engagement angles of three corner rounding approaches are 108.7° , 57.5° , and 31.5° , respectively. Corresponding to the engagement angle, cutting contact relationships under three corner rounding approaches is shown in Fig. 9. Obviously, the material removal amounts during one tooth revolution are different in the three approaches. The method for calculating the amount of material removal in one revolution is deduced below.

If f is the feed rate of the cutter, z is the number of teeth in the cutter, and n is the rpm of the cutter, the feed rate of each cutter tooth is given by

$$f_z = f / (nz) \tag{2}$$

The chip thickness t_x at any section X is given by

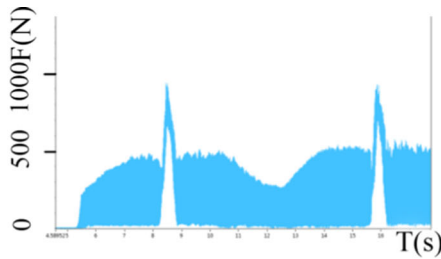
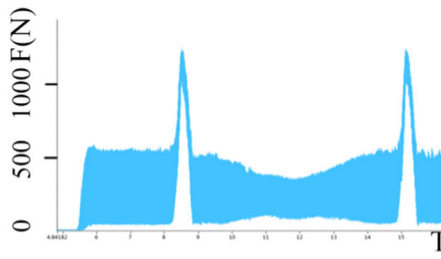
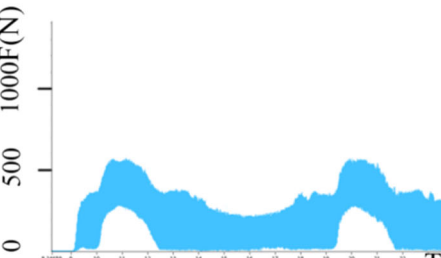
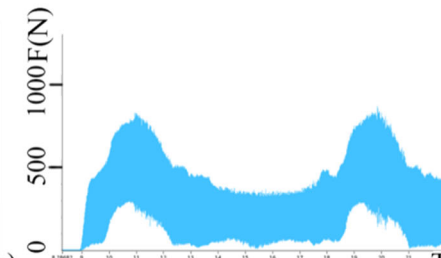
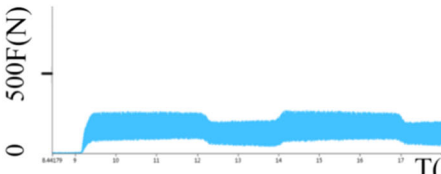
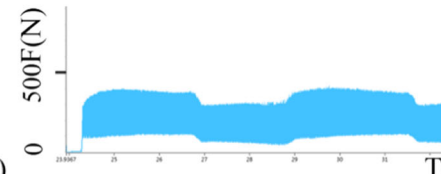
$$t_x = f_z \sin\theta \tag{3}$$

For approach B and approach C, the maximum chip thickness will occur when the angle θ becomes α . For approach A, the maximum chip thickness is f_z .

The mean area of cross section of the chip can be specified by

$$\begin{aligned} A_{mean} &= \int_0^\alpha \frac{1}{2} (t_x)^2 d\theta = \int_0^\alpha \frac{1}{2} (f_z \sin\theta)^2 d\theta \\ &= \frac{1}{8} f_z^2 (2\alpha - \sin 2\alpha) \end{aligned} \tag{4}$$

Table 3 Comparison of corner milling forces in different corner rounding approaches

Factor A (different corner rounding radius approaches)	Factor B (axial cutting depth A_p , mm)	
	$A_p = 7\text{mm}$	$A_p = 12\text{mm}$
Approach A ($r=1\text{mm}$)		
Approach B ($r=8\text{mm}$)		
Approach C ($r=25\text{mm}$)		

And the corresponding cutting time is

$$T_{time} = \frac{60}{n} \frac{\alpha}{2\pi} = \frac{30\alpha}{\pi n} \tag{5}$$

According to the above formulas, a series of calculations are carried out for the three corner approaches. The results of mean areas are $A_{\text{mean-A}} = 344.1 \mu\text{m}^2$, $A_{\text{mean-B}} = 86.2 \mu\text{m}^2$, and $A_{\text{mean-C}} = 16.3 \mu\text{m}^2$ respectively. The results of cutting times are $T_{\text{time-A}} = 2.26 \text{ ms}$, $T_{\text{time-B}} = 1.20 \text{ ms}$, and $T_{\text{time-C}} = 0.66 \text{ ms}$ respectively. Furthermore, the material removal rates ($A_{\text{mean-A}}/T_{\text{time-A}}$) can be calculated and the results of the three corner

rounding approaches are 152.3, 71.8, and 24.7 $\mu\text{m}^2/\text{ms}$ respectively. Therefore, the material removal quantities and material removal rates of three approaches are quite different. This is the main reason for the large difference in milling force as shown in Table 3.

The difference in the milling force will be further analyzed by means of a force balance model of chip formation of orthogonal cutting (Fig. 10). There are three groups of forces in the model. The cutting force F_t and the thrust force F_f produce the resultant force F . The resultant force F is balanced by an equal and opposite force along the shear plane and is resolved into a shear force F_s and a normal force F_n [27].

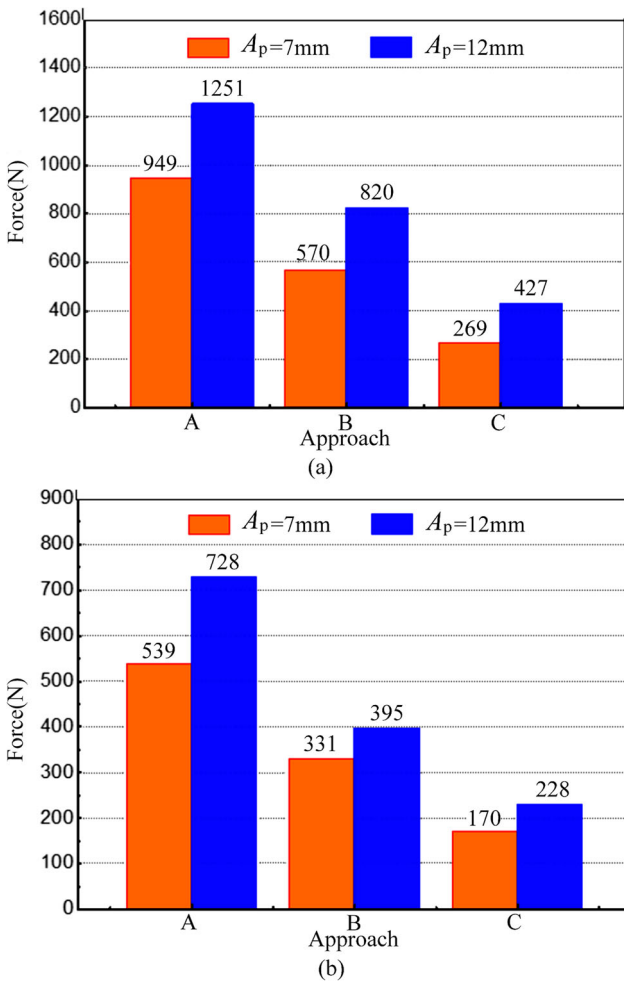


Fig. 8 Comparison of milling forces at corners in three approaches: **a** comparison of maximum milling forces and **b** comparison of average milling forces

$$F_s = F_t \cos\phi - F_f \sin\phi \tag{6}$$

$$F_n = F_t \sin\phi - F_f \cos\phi \tag{7}$$

The resultant force F is balanced by an equal and opposite force along the rake face of the cutter and is resolved into a friction force F_u and a normal force F_v .

$$F_u = F_t \sin\alpha_r + F_f \cos\alpha_r \tag{8}$$

$$F_v = F_t \cos\alpha_r - F_f \sin\alpha_r \tag{9}$$

Corner rounding approach has a significant impact on milling force. The smaller the corner rounding radius, the greater the material removal amount and material removal rate are, and the more the shear and friction forces will be. If the milling forces F_t , F_f , and F are measured by a force platform at this time, higher milling force values will be obtained in approach A. This is why the approach A in Table 3 has larger milling forces.

In addition, the difference of milling force of different corner rounding approaches can be further analyzed through chip morphology. When the shear and friction forces increase during chip formation, the sawtooth degree of the inner free-form surface of chip generally will increase too.

The sawtooth thickness is given by

$$H_p = H + (H-h_1)/2 \tag{10}$$

The deformation coefficient of sawtooth chip can be calculated with the following formula

$$\xi = \frac{h_1 + (H-h_1)/2}{h} \tag{11}$$

where h is the radial depth of cut.

Since h is varied during milling process, it may be better to use the following calculation formula to evaluate the deformation degree of sawtooth chip [25].

$$G_s = \frac{H-h_1}{H} \tag{12}$$

Considering the chip thickness is gradually reduced during tool tooth cuts into and out contact with workpiece in down milling, the thicker part of chip section will be selected for measurement and analysis. The chip sections of three corner rounding approaches are shown in Fig. 11. According to the above formulas, the chip thicknesses H_p under three corner rounding approaches are 297, 231, and 175 μm respectively, and the deformation degrees G_s are 0.334, 0.301, and 0.284 respectively.

It is worth mentioning that the deformation degree of sawtooth chip can also be analyzed by a new method of micro 3D scanning. In Fig. 12, the roughness of the inner free-form surface of chip has been measured via the cross-section on the 3D scanning data. The roughness values R_z of three corner rounding approaches are 9.2, 5.82, and 3.66 μm respectively. This is closely related to higher milling forces in the chip formation process.

In short, the above analyses about material removal rate, force balance, and chip formation indicate corner rounding approach have a signification impact on milling force and chip morphology. More shear and friction forces and cutting heat will generate in the smaller corner rounding approach, and these changes may lead to faster tool wear.

3.2.2 Milling temperature

The results in Fig. 9 are obtained by comparing and analyzing tool temperatures in the three corner cutting approaches with the axial cutting depth of $A_p = 12\text{mm}$. The temperature changing rule with the axial cutting depth of $A_p = 7\text{mm}$ is similar. The cutting temperature keeps rising and reaches the peak

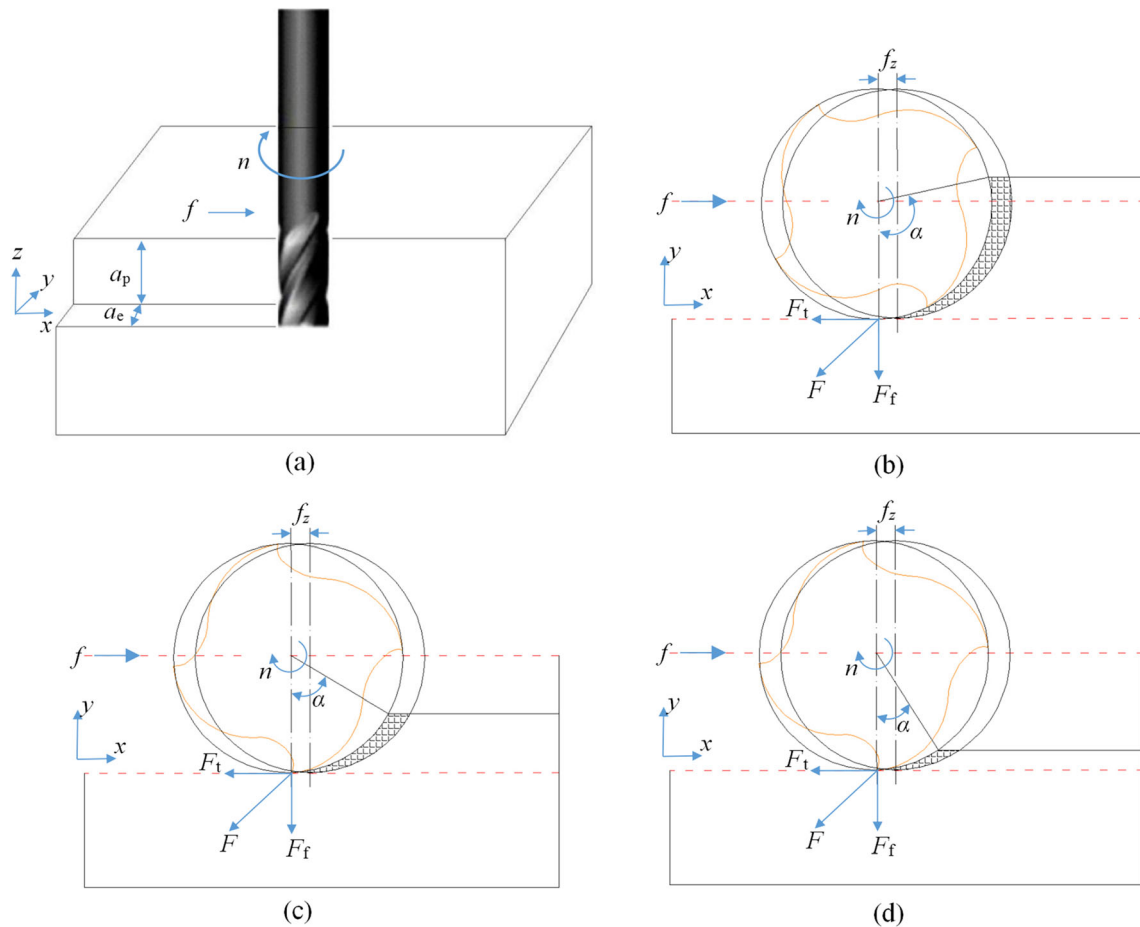


Fig. 9 Cutting contact relationships of three corner rounding approaches: **a** cutting process between tool and workpiece, **b** approach A, **c** approaches B, and **d** approaches C

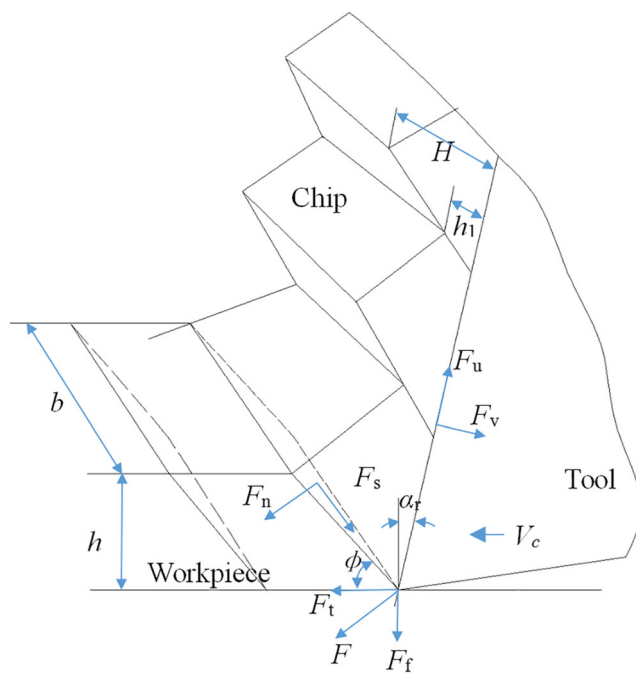


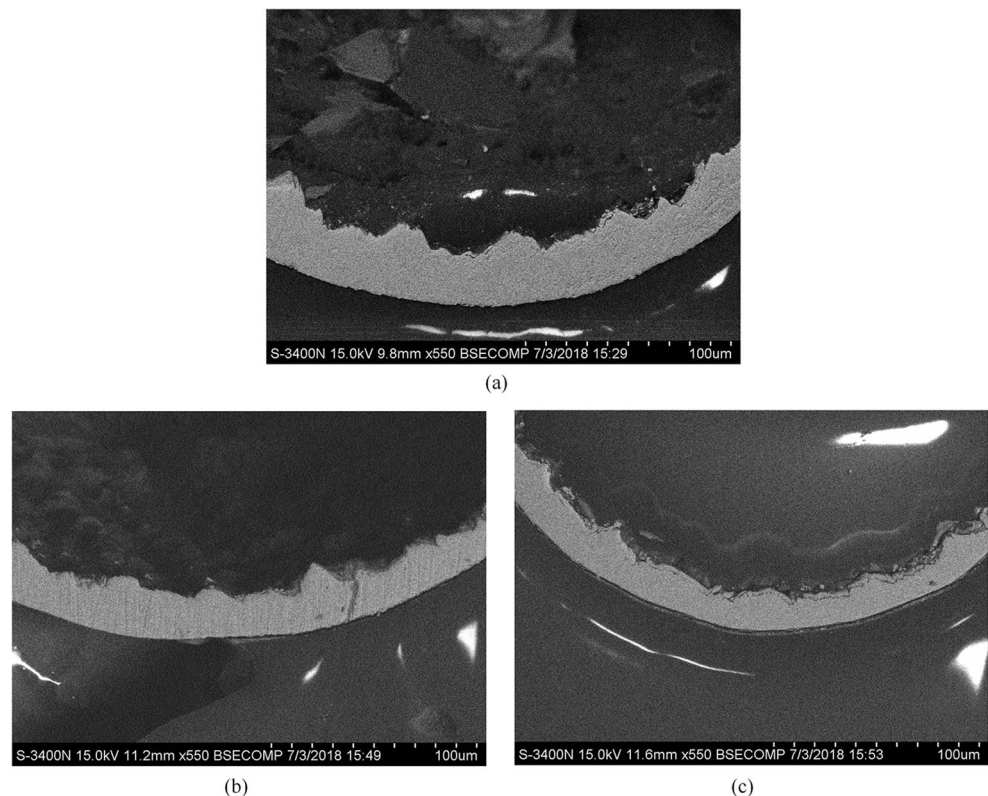
Fig. 10 Sawtooth chip and cutting forces in the chip formation process

after cutting in each corner; and then, the cutting temperature drops gradually after cutting out this corner.

The histogram of Fig. 14 is drawn according to the peak temperature data in a, b, and c of Fig. 13. It shows that the corner rounding approach has significant influence on temperature. The larger the corner rounding radius at corner is, the lower the milling temperature will be. In addition, increase of axial cutting depth may also lead to certain temperature rise.

The above suggests that changing corner rounding approach may lower cutting temperature effectively. According to Dolinšek et al. [11], high tool-chip interface temperature, increased thermal dynamical friction, and intensified oxidation and element diffusion are highly possible in the cutting and high-speed milling of hard material. In the hardened steel milling research by Wang et al. [14], the material is hard, the cutting speed is high, and the tool-chip contact is long, which is likely to cause high cutting temperature and tool stress and intensify oxidation wear and diffusion wear of the tool. The experiment condition in this paper is high-speed deep milling of hardened steel with a larger cutting depth, and the radial cutting depth in corner milling is variable. A sudden increase in material amount in the corner cutting of a small corner

Fig. 11 Sawtooth morphologies of three corner rounding approaches: **a** approach A, $H_p = 297 \mu\text{m}$, $G_s = 0.334$; **b** approach B, $H_p = 231 \mu\text{m}$, $G_s = 0.301$; and **c** approach C, $H_p = 175 \mu\text{m}$, $G_s = 0.284$



rounding radius may lead to great shear force of chip, obvious increase in tool-chip contact length, and severe friction between tool and chip as well as between tool and workpiece, which may lead to sharp temperature rise of tool. The high-speed deep milling temperature exceeds $800 \text{ }^\circ\text{C}$ for a small corner rounding radius. Since the average temperature in the milling area is measured by thermal infrared imager, the actual peak temperature may be a little higher. Therefore, it will affect tool wear significantly. The tool-chip contact length, friction force, and shear force can be reduced effectively by increasing corner rounding radius, through which, less cutting heat is generated, and cutting temperature is lowered finally.

In addition, it is worth mentioning that the higher temperature will cause the workpiece softening effect and reduce the milling force [28]. But from the above force analysis, the milling force of the small corner rounding mode is still far higher than the big corner rounding mode, which indicates that the high temperature thermal softening effect on the milling force of corner deep milling is not obvious.

3.3 Tool wear mechanism of deep milling of hardened steel in the non-steady cutting state

Tool wear mechanism is studied on the basis of the machining and test results of three approaches with the axial cutting depth of $A_p = 12 \text{ mm}$ (similar conclusion can be drawn with the axial cutting depth of $A_p = 7 \text{ mm}$). Scanning electron microscopy

(SEM) is made for the tool flank when it cuts to 130 cm^3 in three approaches (A, B, and C) respectively, and the detection results are shown as Fig. 15. The following conclusions can be drawn in combination with Fig. 7b wear curve: approach A (Fig. 15a) corresponds to the rapid wear stage of tool wear curve, approach B (Fig. 15b) corresponds to the late period of the stable wear stage, and approach C (Fig. 15c) corresponds to the early period of the stable wear stage.

(1) Abrasive wear

In high-speed milling, abrasive wear is an important way of tool wear. Oliveira and Diniz [29] concluded that the tool wear was caused mainly by abrasive wear at the beginning of tool life. For high-speed deep milling of hardened steel, abrasive wear is the main wear form in the early stage of tool wear, too. Due to the frictional contact between workpiece and tool, hard carbide alloy particles may cause the formation of grooves on the tool surface.

Abrasive wear is one of the major wear forms at the stable wear stage in high-speed deep milling of hardened steel. Obvious groove and notch can be seen on the tool flank at the stable wear stage shown as Fig. 15b and Fig. 15c, which is the result of abrasive wear. The paper of Dolinšek et al. [11] indicates that Al_2O_3 and complex mixed oxides, like $(\text{Al}, \text{Ti})_x\text{O}_y$, may be generated by the oxygen element in air and the workpiece and chip in the case of high temperature of tool-

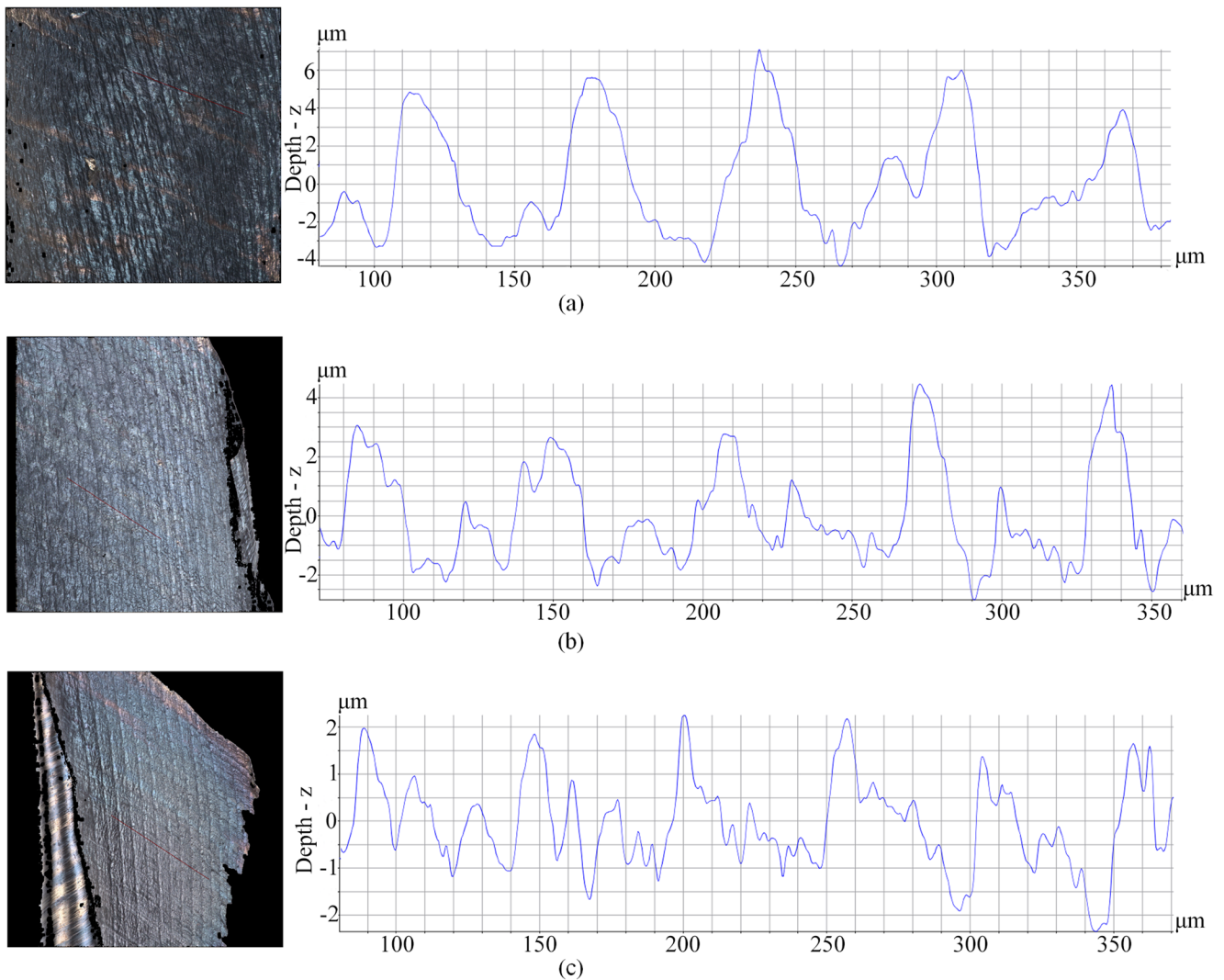


Fig. 12 Sawtooth chip morphologies and section curves under three corner rounding approaches: **a** approach A, $R_z = 9.2 \mu\text{m}$, $R_a = 2.44 \mu\text{m}$; **b** approach B, $R_z = 5.82 \mu\text{m}$, $R_a = 1.34 \mu\text{m}$; and **c** approach C, $R_z = 3.66 \mu\text{m}$, $R_a = 0.74 \mu\text{m}$

chip contact area, and hard oxide particles can cause obvious abrasive wear on the surface of the tool. In addition, the temperature measurement results in Fig. 14 show that the cutting temperature is high in corner machining. O and Fe can be detected in the adhesive bulge of Fig. 15b, c, which indicates high temperature in cutting. Hard oxide particles are easily generated under high temperature, which enhances the abrasive wear effect further.

Adhesive wear is dominant at the rapid tool wear stage. A large amount of adhesive substance can be seen in Fig. 15a, while the groove and notch caused by abrasive wear are not that obvious in most cases.

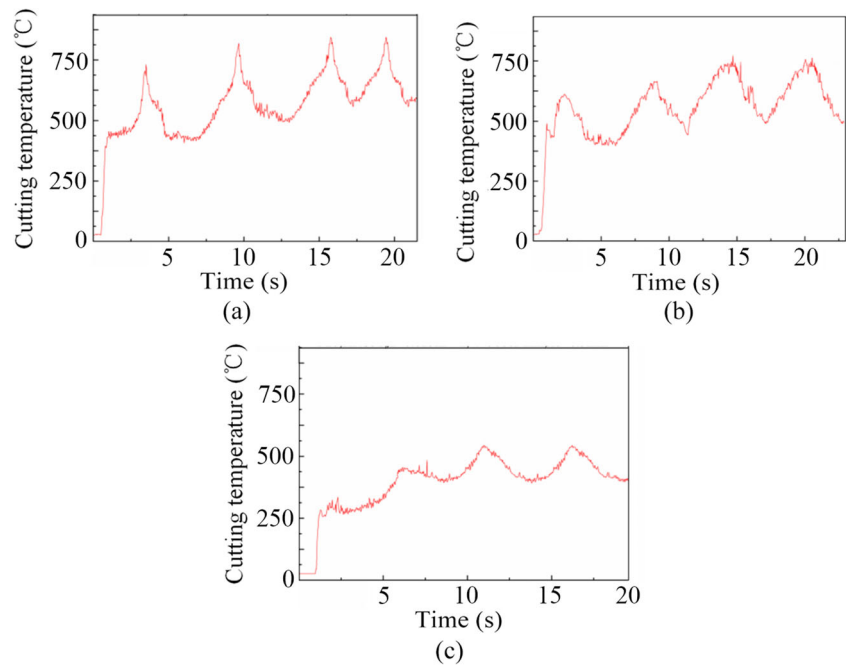
(2) Adhesive wear

Adhesive wear is one of the main wear forms in end milling, which can be seen in the researches of Koshy et al. [30]

and Nouari and Ginting [31]. Due to the high temperature and high pressure between chip and cutting edge in the high-speed deep milling of hardened steel, chip is likely to stick to cutting edge, and adhesion and seaming may occur. The workpiece material sticking to the tool flank may peel off due to collision, friction, tearing, etc. Tool coating is damaged in the processes above, and tool coating material may be brought away by falling materials, which will lead to exposure of tool substrate.

Serious adhesive wear is likely to occur at the rapid wear stage. The tool in Fig. 15a (approach A) is at rapid wear stage, where a large amount of bulges and some pits are formed on the cutting edge and in the surrounding area. A great amount of Fe is discovered through energy spectrum analysis for the bulge at position B, which indicates adhesion and even seaming of chip. Besides, a certain amount of O is discovered, which shows a high cutting temperature. A large number of tool carbide substrate elements—C, W, and Co—are

Fig. 13 Tool temperatures in three corner cutting approaches with the axial cutting depth of 12 mm: **a** approach A, **b** approach B, and **c** approach C



discovered in the energy spectrum analysis for the pit C around the cutting edge in Fig. 15a, which suggests that the tool coating has been brought away after friction, tearing and falling of seaming and adhesive material, and the tool substrate has been exposed.

Adhesive wear is not obvious at the early tool wear stage. Adhesive wear appears and increases gradually with cutting at the stable tool wear stage. Figure 15b (approach B) and Figure 15c (approach C) correspond to different periods at the stable tool wear stage. The number of bulges on the cutting edge in Fig. 15b is less than that in Fig. 15a, and there is a part

of coating material left in the pit formed. The number of bulges on the cutting edge in Fig. 15c is less than that in Fig. 15b, and a lot of tool coating materials still can be detected in the pit formed.

(3) Oxidative wear

Tool and tool coating material will react with O element in air after exceeding certain temperature in the high-speed deep milling of hardened steel, which will accelerate tool wear.

At the rapid tool wear stage, the O element in air may react with the Ti and Al in tool coating, or the Fe in chip adhesive material, or the C, etc. in tool substrate due to very high cutting temperature, which will accelerate tool wear. Figure 15c (approach A) corresponds to rapid wear stage. O is detected in energy spectrum analysis at points A, B, and C in the cutting edge area. Point A is the tool nose area of the cutting edge, where tool coating turns invalid, and the carbide substrate is exposed. Besides, a great amount of O is detected with an atomic percentage of about 48.01%. Point B is the chip adhesive area, where a great amount of O is detected with an atomic percentage of about 52.29%. Point C is a pit formed after peeling of chip adhesive material, where tool substrate is exposed and a small amount of O element is detected.

Oxidative wear increases gradually along with the cutting progress at the stable tool wear stage. O element is detected at corresponding positions of the cutting edge in Fig. 15b (approach B) and Fig. 15c (approach C) corresponding to different periods at the stable wear stage. Figure 15c corresponds to the early period of the stable wear stage, when the content of O at various positions of the cutting edge is little, which indicates

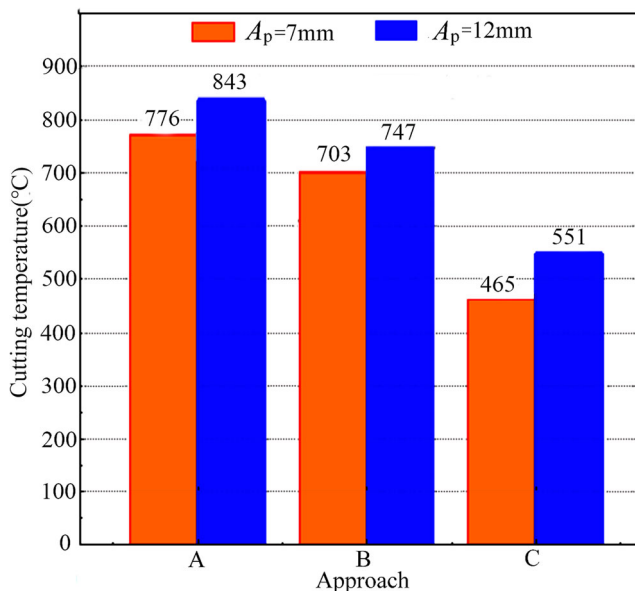
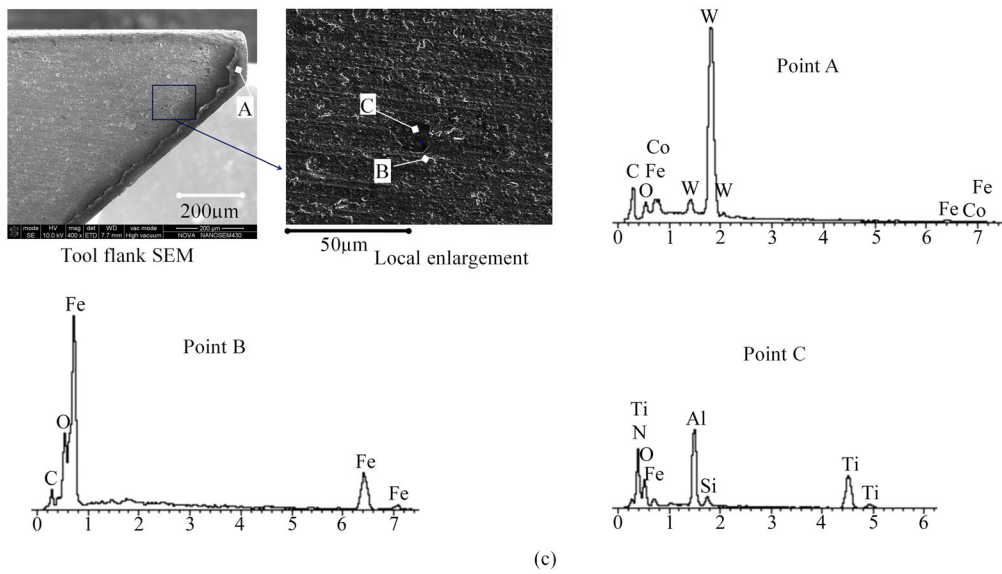
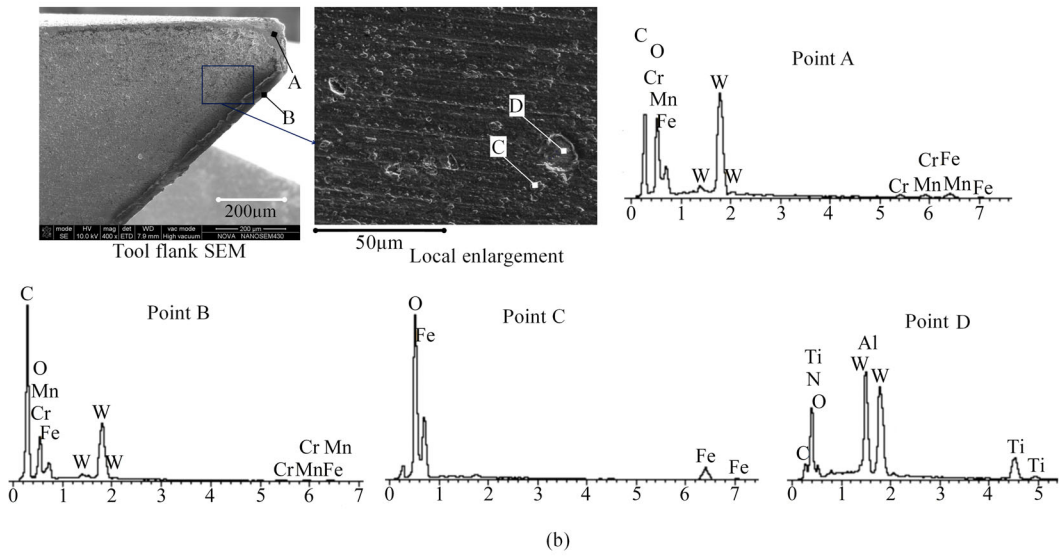
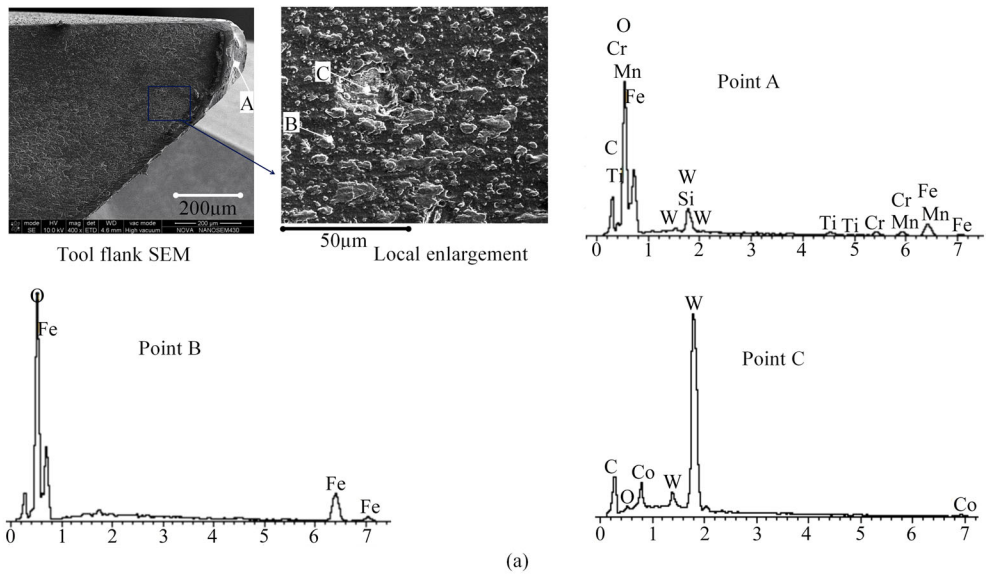


Fig. 14 Comparison of tool temperatures in three corner cutting approaches



◀ **Fig. 15** SEM of three corner rounding approaches ($A_p = 12$ mm): **a** approach A (late period of rapid wear stage of wear curve), **b** approach B (late period of stable wear stage of wear curve), and **c** approach C (early period of stable wear stage of wear curve)

a minor oxidative wear degree. Figure 15b corresponds to the late period of the stable wear stage, when the content of O at various positions of the cutting edge is greater than that in Fig. 15a and less than that in Fig. 15c, which indicates an oxidative wear degree between them.

(4) Diffusion wear

In the cutting process, some elements will diffuse from one area to another under certain temperature and cause diffusion wear. Diffusion wear may lead to change in tool coating or carbide substrate and reduce the cutting performance of the tool.

Diffusion wear is obvious at rapid tool wear stage. According to Wang et al. [14], Co diffusion is likely to occur when the cutting temperature exceeds 800 °C. Moreover, based on Haron et al. [32], Co in alloy tool will be dissolved and diffuse into chip due to high temperature after coating peeling. Co loss may lead to decrease in tool strength, and it is also an important cause for slight tipping, crack, and tool breakage. The wear status of the tool nose on the tool flank in Fig. 15a (approach A) and the energy spectrum result of point A show that the coating has peeled off and the carbide substrate is exposed. A certain amount of elements in workpiece material, i.e., Fe, Mn, and Cr (atomic percentage accounts for 36.04% approximately), are detected at point A, and there is little Co in the carbide substrate. Such phenomena indicate serious diffusion, which may intensify tool wear. The tool substrate contacts the chip/workpiece directly when the coating peels off. The Co in carbide substrate will diffuse when the cutting temperature exceeds a certain limit, which may reduce the strength of tool substrate and accelerate tool wear. The tool nose in Fig. 15a is subject to very serious wear and slight tipping, which is closely related to diffusion wear.

Diffusion wear also can be seen at stable tool wear stage, which increases gradually along with cutting progress. The wear status of the tool nose in Fig. 15c (approach C) and the energy spectrum analysis result show that the coating has peeled off and little Fe and a certain amount of Co are present, which suggests slight diffusion wear. The wear status of the tool nose in Fig. 15b (approach B) and the energy spectrum analysis result show that the coating has peeled off, very little Co is present, and the amount of Fe is between that in approach A and approach C, which also indicates slight diffusion wear in a degree between that in approach A and approach C.

3.4 Impact on tool wear in deep milling of hardened steel from corner rounding approach and cutting depth

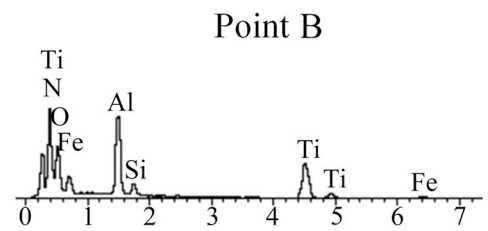
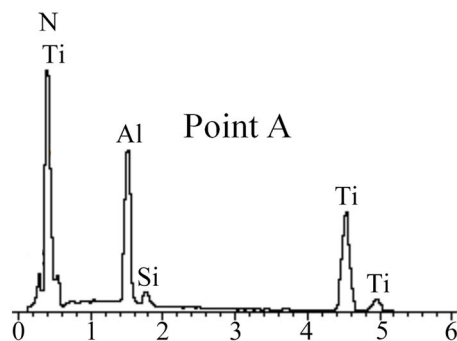
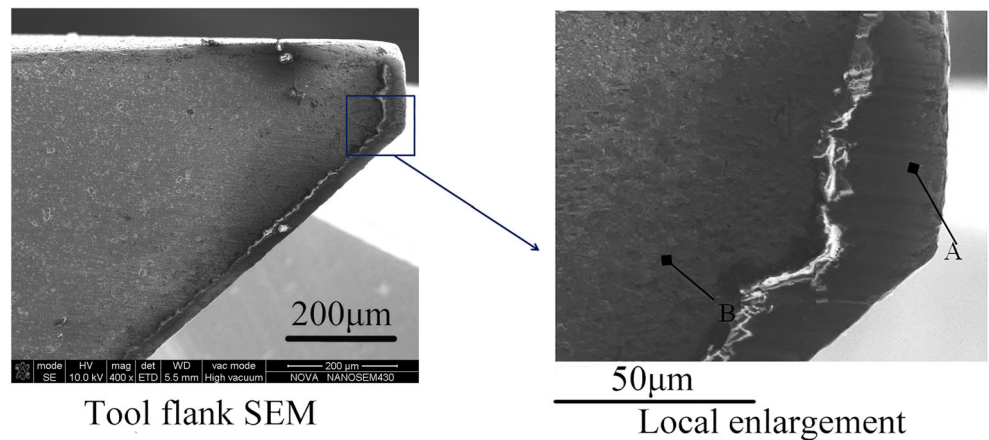
First of all, Table 4 is obtained by sorting out the contrast analysis results of the tool wear in the three corner rounding approaches based on the SEM results in Fig. 15. It can be learnt from Table 4 that if stable wear stage and rapid wear stage come early in the deep milling with small corner rounding radius, serious adhesion, diffusion and oxidation wear, as well as tool tipping are very likely to occur. However, tool wear and breakage degrees drop significantly when the tool rounding radius keeps increasing. According to Venugopal et al. [33], rapid wear and failure of tool are closely related to adhesion-dissolution-diffusion, and higher tool temperature will accelerate wear and failure of tool. Furthermore, according to Machado et al. [15], milling is a kind of intermittent cutting. Great temperature difference exists and thermal fatigue is generated in each rotation cycle of tool, and the cut-in and cut-out of cutting edge cause mechanical shock. Such two factors will lead to increase in tool wear in hardened steel machining, and chipping and cutting-edge breakage are likely to occur. It is proved in the temperature and milling force analyzes above that corner rounding approach has significant impact on force and temperature. It is likely to generate high tool-chip interface temperature and great tool load in the high-speed deep milling with a small corner rounding radius. In this case, the cutting edge is under greater thermal fatigue and mechanical shock. Thermal power is enhanced under high temperature, which will intensify oxidation wear and abrasion wear. In addition, adhesion wear and diffusion wear between tool and chip are likely to occur and be intensified under high temperature and high pressure. The wear forms above will lead to rapid wear and peeling of tool coating, and tool wear progress will be accelerated further when the substrate is exposed. Furthermore, Co diffusion, thermal fatigue, and strong mechanical shock are very likely to cause tool damages, such as chipping and tipping at tool nose, etc. of cutting edge. Tool temperature and load in corner deep milling can be controlled effectively by increasing the corner rounding radius, which is beneficial to protecting tool coating and substrate, delaying tool wear progress and preventing tool breakage.

Figure 16 shows the tool flank wear in corner approach C under the axial cutting depth of 7 mm. Compared with Fig. 15c (axial cutting depth $A_p = 12$ mm), the adhesion, oxidation, and diffusion wear of tool are reduced to a certain extent, and the coating peeling, etc. of tool nose is alleviated effectively. The main reasons are that the maximum milling force and the average milling force under the axial cutting depth of 7 mm are obviously lower than that under the axial cutting depth of 12 mm, and the milling temperature drops to some extent. During deep milling of hardened steel, reducing the axial cutting depth can reduce tool wear and breakage to a certain extent, but the machining efficiency will be reduced.

Table 4 Comparison results of tool flank wear in three corner rounding approaches

Corner rounding approach	Tool nose	Cutting edge
Approach A ($r = 1$ mm)	With the most serious wear degree in the three approaches. Serious tipping occurs. Tool substrate is exposed since coating has been worn and peeled off. A large number of grooves caused by abrasive wear occur. Serious oxidative wear (atomic percentage of O accounts for 48.01% approximately) and diffusion wear (atomic percentage of elements of work-piece material, such as Fe, Mn and Cr, accounts for 36.04% approximately) have emerged.	Tool flank has the poorest surface quality. Lots of cohesive bulges and pits are formed. The bulge is the workpiece material subject to adhesion, seaming, and serious oxidation (atomic percentage of O accounts for 52.29% approximately); carbide tool substrate is exposed and oxidized at the pit, but no coating element is discovered at the pit bottom.
Approach B ($r = 8$ mm)	The wear degree is lower than that in approach A. Local tipping occurs, obvious coating peeling occurs at tool nose, and tool substrate is exposed. Grooves caused by abrasive wear are less obvious than that in approach A. Obvious oxidation wear (atomic percentage of O accounts for 34.18% approximately) and diffusion wear (atomic percentage of elements of workpiece material, such as Fe, Mn, and Cr, accounts for 28.02% approximately) have emerged.	The surface quality of tool flank is better than that in approach A. A certain amount of cohesive bulges and pits are formed, and the adhesive wear is lighter than that in approach A. The bulge is the workpiece material subject to adhesion, seaming, and obvious oxidation (atomic percentage of O accounts for 40.22% approximately). Carbide tool substrate is exposed and oxidized at the pit, but there is still some coating at the pit bottom.
Approach C ($r = 25$ mm)	The wear degree is notably better than that in approach A and approach B. No obvious tipping is discovered, and the grooves caused by abrasive wear are less obvious than that in approach B. Tool substrate is exposed. Slight oxidation wear (atomic percentage of O accounts for 11.43% approximately) and diffusion wear (atomic percentage of elements of work-piece material like Fe accounts for 5.99% approximately) have emerged.	The surface quality of tool flank is better than that in approach B. A small number of bulges and pits are formed, and the adhesive wear is lighter than that in approach A and approach B. The bulge is the workpiece material subject to adhesion, seaming, and little oxidation (atomic percentage of O accounts for 16.09% approximately). There is still a lot of coating at the pit, but no substrate is exposed.

Fig. 16 Tool flank wear in corner approach C under the axial cutting depth of 7 mm



4 Conclusions

Continuous deep milling experiments with different corner rounding approaches are designed to study the tool wearing process and mechanism for hardened steel mold pocket, and conclusions are as follows:

- (1) In small corner rounding approach, the stable wear stage is very short; the tool transits from the initial wear stage to the rapid wear stage very soon with a short life. In medium corner rounding approach, the stable wear stage is relatively longer, and the final tool life is longer to a certain extent. Compared with the two approaches above, in large corner rounding approach, the slope at initial wear and rapid wear stages is smaller, while the stable wear stage is longer, and the tool life is improved obviously.
- (2) Corner rounding approach has a significant impact on milling force, which is the leading factor for the change in milling force. The smaller the corner rounding radius, the greater the material cutting amount and the larger the engagement angle is, the more the infinitesimal forces (shear and friction forces) will be, and thus lead to dramatic increase of tool load. Corner rounding approach has an obvious influence on cutting temperature, thus cutting temperature can be reduced effectively by increasing corner rounding radius. Besides, axial cutting depth also has certain significant impact on cutting temperature.
- (3) Abrasive wear is a major wear form at the initial tool wear stage in high-speed deep milling of hardened steel. Adhesive wear and oxidative wear appear and increase gradually with cutting at the stable tool wear stage, and get worse at the rapid wear stage. Adhesive wear and oxidative wear will intensify wear and peeling of tool coating further on the basis of abrasive wear. The coating on the tool nose peels off completely first, and the tool strength of this area is reduced further due to diffusion wear, which leads to tool breakages in tool nose area, such as chipping and tipping.
- (4) Corner rounding approach has an extremely obvious impact on the deep milling of hardened steel. It is likely to generate high tool-chip interface temperature and great tool load in high-speed deep milling with small corner rounding radius. In this case, the cutting edge is under great thermal fatigue and mechanical shock. Besides, abrasive wear is severe and adhesive wear and oxidative wear are intensified, which leads to rapid wear and peeling of tool coating. Furthermore, substrate will be weakened and tool wear process will be accelerated further due to diffusion wear and oxidation wear when the substrate is exposed. As a result, the tool nose is very likely to be damaged, such as chipping and tipping. The tool

temperature and load in corner deep milling can be controlled effectively by increasing the corner rounding radius, which is beneficial to protecting tool coating and substrate, delaying tool wear progress, and preventing tool breakage.

Acknowledgements This work reported in this paper is conducted in conjunction with “Guangdong public welfare research and capacity building project (2017A010102011)” and “Guangdong provincial education department project (2015KTSCX028).”

References

1. SX W, Ma W, Li B, Wang CY (2016) Trochoidal machining for the high-speed milling of pockets. *J Mater Process Technol* 233:29–43
2. Choy HS, Chan KW (2003) Modeling cutter swept angle at cornering cut. *Int J CAD/CAM* 3(1):1–12
3. Han X, Tang L (2015) Precise prediction of forces in milling circular corners. *Int J Mach Tools Manuf* 88:184–193
4. Bae SH, Ko K, Kim BH, Choi BK (2003) Automatic feedrate adjustment for pocket machining. *Comput Aided Des* 35(5):495–500
5. Karunakaran KP, Shringi R, Ramamurthi D, Hariharan C (2010) Octree-based NC simulation system for optimization of feed rate in milling using instantaneous force model. *Int J Adv Manuf Technol* 46(5–8):465–490
6. Liu X, Ding YP, Yue C, Zhang R, Tong X (2015) Off-line feedrate optimization with multiple constraints for corner milling of a cavity. *Int J Adv Manuf Technol* 7:1–9
7. Choy H, Chan K (2002) Enhanced strategy for milling corners. *IMEche*, part B. *J Eng Manuf* 16(8):1135–1154
8. Zhao ZY, Wang CY, Zhou HM, Qin Z (2007) Pocketing toolpath optimization for sharp corners. *J Mater Process Technol* 192:175–180
9. Ibaraki S, Yamaji I, Matsubara A (2010) On the removal of critical cutting regions by trochoidal grooving. *Precis Eng* 34(3):467–473
10. Dumitrache A, Borangiu T (2012) IMS10-image-based milling toolpaths with tool engagement control for complex geometry. *Eng Appl Artif Intell* 25(6):1161–1172
11. Dolinšek S, Sustarsic B, Kopac J (2001) Wear mechanisms of cutting tools in high-speed cutting processes. *Wear* 250(1–12):349–356
12. Ghani JA, Choudhury IA, Masjuki HH (2004a) Performance of P10 TiN coated carbide tools when end milling AISI H13 tool steel at high cutting speed. *J Mater Process Technol* 153–154(1):1062–1066
13. YS L, Lin HM, Chen YC (2007) Feasibility study of the minimum quantity lubrication in high-speed end milling of NAK80 hardened steel by coated carbide tool. *Int J Mach Tools Manuf* 47(11):1667–1676
14. CY W, Xie YX, Qin Z, Lin HS, Yuan YH, Wang QM (2015) Wear and breakage of TiAlN- and TiSiN-coated carbide tools during high-speed milling of hardened steel. *Wear* 336–337:29–42
15. ÁR M, Diniz AE (2017) Tool wear analysis in the machining of hardened steels. *Int J Adv Manuf Technol* 92:4095–4109
16. Braghini A, Coelho RT (2001) An investigation of the wear mechanisms of polycrystalline cubic boron nitride (PCBN) tools when end milling hardened steels at low/medium cutting speeds. *Int J Adv Manuf Technol* 17:244–257
17. XB C, Zhao J, Dong YW (2013) The effects of cutting parameters on tool life and wear mechanisms of CBN tool in high-speed face milling of hardened steel. *Int J Adv Manuf Technol* 66:955–964
18. Castanhera IDC, Diniz AE (2016) High speed milling of hardened steel convex surface. *Procedia Manufacturing* 5:220–231
19. Wang CY, Ding F, Tang DW, Zheng LJ, Li SY, Xie YX (2016) Modeling and simulation of the high-speed milling of hardened

- steel SKD11 (62 HRC) based on SHPB technology. *Int J Mach Tool Man* 108:13–26
20. Pu Z, Singh A (2013) High speed ball nose end milling of hardened AISI A2 tool steel with PCBN and coated carbide tools. *J Manuf Process* 15(4):467–473
 21. Wojciechowski S, Maruda RW, Barrans S, Nieslonv P, Krolczyk GM (2017) Optimisation of machining parameters during ball end milling of hardened steel with various surface inclinations. *Measurement* 111:18–28
 22. Wojciechowski S, Maruda RW, Królczyk GM, Niesłony P (2018) Application of signal to noise ratio and grey relational analysis to minimize forces and vibrations during precise ball end milling. *Precis Eng* 51:582–596
 23. Wojciechowski S (2011) Machined surface roughness including cutter displacements in milling of hardened steel. *Metrol Meas Syst* 18(3):429–440
 24. Qin J, Long Y, Zeng J, Wu S (2014) Continuous and varied depth-of-cut turning of gray cast iron by using uncoated and TiN/Al₂O₃ coated silicon nitride-based ceramic tools. *Ceram Int* 40(8):12245–12251
 25. Wang C, Xie Y, Zheng L, Qin Z, Tang D, Song Y (2014) Research on the chip formation mechanism during the high-speed milling of hardened steel. *Int J Mach Tools Manuf* 79(4):31–48
 26. Oxley PLB (1962) An analysis for orthogonal cutting with restricted tool-chip contact. *Int J Mech Sci* 4(2):129–135
 27. Altintas Y (2012) *Manufacturing automation: metal cutting mechanics, machine tool vibrations, and CNC design*. Cambridge university press, Cambridge
 28. Ghani JA, Choudhury IA, Masjuki HH (2004b) Wear mechanism of TiN coated carbide and uncoated cermets tools at high cutting speed applications. *J Mater Process Technol* 153:1067–1073
 29. Oliveira AJD, Dimiz AE (2009) Tool life and tool wear in the semi-finish milling of inclined surfaces. *J Mater Process Technol* 209(14):5448–5455
 30. Koshy P, Dewes RC, Aspinwall DK (2002) High speed end milling of hardened AISI D2 tool steel (~58 HRC). *J Mater Process Technol* 127(2):266–273
 31. Nouari M, Ginting A (2006) Wear characteristics and performance of multi-layer CVD-coated alloyed carbide tool in dry end milling of titanium alloy. *Surf Coat Technol* 200(18–19):5663–5676
 32. Haron CHC, Ginting A, Arshad H (2007) Performance of alloyed uncoated and CVD-coated carbide tools in dry milling of titanium alloy Ti-6242S. *J Mater Process Technol* 185(1–3):77–82
 33. Venugopal KA, Paul S, Chattopadhyay AB (2007) Growth of tool wear in turning of Ti6Al4V alloy under cryogenic cooling. *Wear* 262(9):1071–1078